

Mid- and far-infrared properties of dynamical models of carbon-rich long-period variables

W. Windsteig¹, E.A. Dorfi¹, S. Höfner^{1,2}, J. Hron¹, and F. Kerschbaum¹

¹ Institut für Astronomie der Universität Wien, Türkenschanzstraße 17, A-1180 Wien, Austria

² Niels Bohr Institute, University Observatory, Juliane Maries Vej 30, DK-2100 Copenhagen, Denmark

Received 20 September 1996 / Accepted 3 February 1997

Abstract. We have calculated spectral energy distributions and synthetic IRAS colours of carbon-rich long-period variables. On top of dynamical models for the stellar atmosphere and circumstellar envelope which consistently treat the time-dependent hydrodynamics, the formation of amorphous carbon grains and grey radiative transfer, frequency-dependent radiative transfer calculations have been carried out in the range between $1\ \mu\text{m}$ and $290\ \mu\text{m}$. Calculating the IRAS colours we find that the models lie in regions I (stars without circumstellar shells) and VII (variable stars with carbon-rich circumstellar shells) of the IRAS two colour diagram in accordance with observational results for carbon stars. They form an almost linear sequence (near the black body line) reflecting the different mass loss rates. We compare our results to empirical formulae which link the mass loss rate to the observed flux at $60\ \mu\text{m}$. Furthermore, we have also investigated qualitatively the effects of dust with α -SiC grains and of detached shells. The SiC-contribution causes mainly a blue-shift of about 0.2 mag in the [12]–[25] colour. Adding a detached shell results in higher [25]–[60] values partly shifting the models into region VIa (non-variable stars with relatively cold dust at large distances) of the IRAS two colour diagram as expected from observations.

Key words: stars: AGB and post-AGB – stars: variables – stars: mass-loss – stars: circumstellar matter – stars: carbon – hydrodynamics

1. Introduction

The IRAS satellite has produced the largest (spectro)-photometric data base for AGB stars in the mid- and far-infrared and these data have been the starting point for many investigations on the properties of these stars (see the recent review of Habing 1996). A main tool for analyzing the dust envelopes

Send offprint requests to: W. Windsteig,
(windsteig@auro.ast.univie.ac.at)

around carbon stars has been the modelling of the spectral energy distributions starting with the work of Rowan-Robinson & Harris (1983). The large majority of these modelling efforts used a number of simplifying assumptions like stationary winds, an instantaneous condensation of dust grains with given particle sizes at a certain temperature or distance from the star. Winters et al. (1994a) have applied the description of grain formation and growth developed by Gail & Sedlmayr (1988) and Gauger et al. (1990) to stationary winds and have calculated synthetic IR spectra and IRAS colours.

Time-dependent hydrodynamical simulations of the atmospheres of carbon-rich long-period variables (LPVs) have demonstrated the strong interaction of dust formation and gas dynamics in these stars (e.g. Fleischer et al. 1991, 1992, 1995, Höfner et al. 1995, 1996, Höfner & Dorfi 1997) and Winters et al. (1994b, 1995) have calculated the corresponding theoretical IR light curves as well as brightness profiles. These investigations reveal the complex structure of dust shells caused by shock waves and study the time-dependence of the inner parts of the circumstellar envelope. Since the dust forming zones of LPVs never develop into a stationary state the synthesis of spectra of carbon-rich LPVs also demands a careful treatment of the hydrodynamics together with the time-dependent dust formation process.

Our current paper deals with the mid- and far-infrared properties of a number of dynamical models of carbon-rich LPVs. The IRAS colours, the corresponding IRAS LRS classes as well as a relation between the mass loss rate and the $60\ \mu\text{m}$ flux are presented for dynamical models of circumstellar shells. These results are based on accurate numerical solutions of radiation hydrodynamics interacting with time-dependent dust formation and growth processes where the optical constants of the amorphous carbon grains (and SiC particles) are taken from laboratory data.

In Sect. 2 we briefly describe the physical and numerical input, Sect. 3 deals with the synthetic spectral energy distributions as well as the IRAS two colour diagram and is followed by the LRS classes of our models in Sect. 4 and by a discussion in Sect. 5.

2. Modelling method

2.1. Dynamical models

The results presented in this paper are based on self-consistent time-dependent models of the atmosphere and circumstellar envelope of LPVs. The models are obtained by solving the system of grey radiation hydrodynamics (describing the energy and momentum balance of gas and radiation) together with a detailed treatment of dust condensation. Considering a carbon-rich environment we assume the formation of amorphous carbon grains (Gail & Sedlmayr 1988, Gauger et al. 1990). The effects of stellar pulsation are included in the calculations by applying a piston accompanied by a variable luminosity at the inner boundary which is located below the stellar photosphere. A thorough description of the dynamical models actually used in this paper (cf. Table 1, model series R and model P5) together with a discussion of the corresponding parameters is given in Höfner & Dorfi (1997). In addition, we have included a few stationary wind models which have been taken from earlier publications (VS: Höfner et al. 1996, L12: Dorfi & Höfner 1996, A23 and B19: Höfner et al. 1995).

The models are determined by the following set of parameters: stellar mass M_* , luminosity L_* and effective temperature T_* of the hydrostatic initial model, carbon-to-oxygen abundance ratio $\varepsilon_C/\varepsilon_O$ as well as the piston parameters period P and velocity amplitude Δu_p . The dynamical calculations yield the spatial structure of the circumstellar envelope (density, velocity, temperature, degree of condensation, mean grain size, etc.) as a function of time as well as average quantities characterizing the outflow like the mass loss rate \dot{M} , outflow velocity u_∞ and the dust-to-gas mass ratio ρ_d/ρ_g .

In the context of IR properties a point of great significance is the spatial extension of the models. All relevant physical phenomena which determine the dynamics of the outflow are concentrated within a spatial region close to the star and are fully covered by the self-consistent calculations. However, to obtain realistic spectral energy distributions it is necessary to consider the entire circumstellar envelope because the extended circumstellar dust shell around the star contributes significantly to the observed IR fluxes causing an infrared excess. As the wind acceleration and the temporal variations affecting the dust-driven wind are essentially restricted to a region within a few photospheric radii we can assume a constant velocity outside our computational outer boundary, typically located at about $30 R_*$. At this point the variability of the outflow velocity is already small compared to the average value (less than 10%). Since it is quite evident that the far-IR emission comes from a spatially very large region, we characterize the outer envelope by mean values of the mass loss rate and outflow velocity averaged over many pulsational cycles. As the deviations of the density and dust-to-gas ratio from the time-average values occur on spatial scales much smaller than the characteristic dimensions for temperature changes it is sufficient to take temporal mean values for the purpose of radiative transfer calculations. From the hydrodynamical calculations we obtain these time-averages of mass loss, degree of condensation and outflow velocity and use them

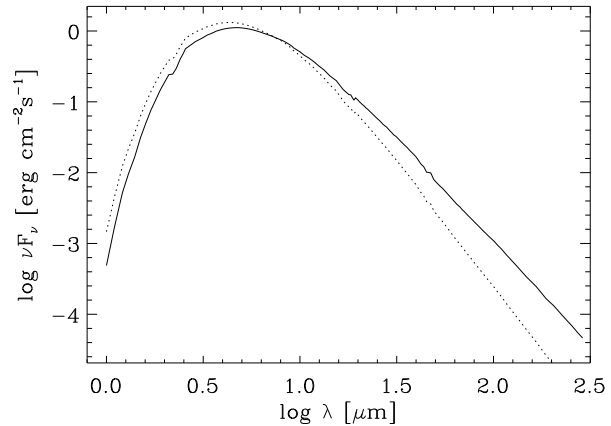


Fig. 1. Infrared excess of model R10C18 based on pure amorphous carbon grains: The full line shows the SED of the extended model ($84000 R_*$), the dotted line corresponds to the model of the dynamical calculations ($22 R_*$).

to determine the density, dust-to-gas ratio and velocity of the expanding circumstellar envelope up to about $10^5 R_*$. At such large radii the temperature can be accurately determined by the Lucy approximation (Lucy 1971, 1976).

2.2. Frequency-dependent radiative transfer

The dynamical models are calculated with a grey approximation of radiative transfer where the corresponding Rosseland mean of the frequency-dependent dust opacities is used. To obtain spectral energy distributions we solve independently for each frequency the time-independent radiative transfer equation along parallel rays (Yorke 1980). The gas opacity is taken from the dynamical models and the dust opacity is calculated from the optical properties given by Maron (1990) for amorphous carbon and by Pégourié (1988) for SiC adopting the small particle limit of the Mie theory (grain sizes are typically between $0.01 \mu\text{m}$ and $0.1 \mu\text{m}$).

3. IRAS two-colour diagram: dynamical models and observations

3.1. Spectral energy distributions

Fig. 1 shows a typical spectral energy distribution (SED) based on pure amorphous carbon grains where the full line represents the extended version of model R10C18 and the dotted line depicts the original dynamical calculation (cf. Table 1 for the model parameters). The comparison clearly illustrates how the infrared excess caused by the dust envelope leads to a significant shift in the IRAS two colour diagram and demonstrates the influence of the size of the circumstellar dust shell on the far-IR emission.

Moreover, the analysis of mid-IR carbon star spectra indicates that α -SiC is the best candidate to reproduce the astronomical observations around the $10 \mu\text{m}$ region (Groenewegen 1995, Speck et al. 1996). Therefore it is plausible to consider

Table 1. Parameters of dynamical models (L_* , M_* , T_* , $\varepsilon_C/\varepsilon_O$, P , Δu_p) and resulting outflow characteristics (mass loss rate \dot{M} , velocity at the outer boundary u_∞ , the dust-to-gas mass ratio ρ_d/ρ_g , the mean radius $R_{2/3}$ where the optical depth becomes $\tau = 2/3$ at $12 \mu\text{m}$, the mean optical depth of the dust envelope τ_d at $12 \mu\text{m}$ and the mean flux-weighted optical depth τ_F). The first group of models consists of LPV envelopes presented in Höfner & Dorfi (1997), the second group contains stationary wind models taken from various other papers. See text for details.

model	L_* [L_\odot]	M_* [M_\odot]	T_* [K]	$\varepsilon_C/\varepsilon_O$	P [d]	Δu_p [km s^{-1}]	\dot{M} [$M_\odot \text{ yr}^{-1}$]	u_∞ [km s^{-1}]	ρ_d/ρ_g [10^{-3}]	$R_{2/3}$ [R_*]	τ_d	τ_F
P5	10000	1.0	2745	1.80	650	2.0	$1.0 \cdot 10^{-5}$	25	3.6	2.2	0.72	1.59
R7C18	7000	1.0	2880	1.80	390	2.0	$5.8 \cdot 10^{-7}$	7	1.7	1.0	0.15	0.67
R10C18	10000	1.0	2790	1.80	525	2.0	$1.6 \cdot 10^{-5}$	25	3.2	4.0	1.1	1.98
R10C15	10000	1.0	2790	1.50	525	2.0	$2.8 \cdot 10^{-6}$	5	1.2	1.3	0.44	1.26
R13	13000	1.0	2700	1.40	650	2.0	$5.9 \cdot 10^{-6}$	7	1.0	1.7	0.56	1.45
R13U	13000	1.0	2700	1.40	650	6.0	$4.5 \cdot 10^{-5}$	13	1.4	5.5	1.3	2.04
R13MU	13000	0.9	2700	1.40	650	6.0	$8.3 \cdot 10^{-5}$	15	1.6	12.0	2.6	3.08
VS	10000	1.0	2600	2.30	–	–	$2.9 \cdot 10^{-7}$	12	1.5	1.0	0.029	0.15
L12	12000	1.0	2600	2.00	–	–	$3.8 \cdot 10^{-7}$	9	1.1	1.0	0.034	0.17
A23	10000	1.0	2600	2.30	–	–	$3.0 \cdot 10^{-7}$	14	1.2	1.0	0.022	0.12
B19	10000	1.0	2500	1.90	–	–	$4.9 \cdot 10^{-7}$	9	1.0	1.0	0.045	0.22

α -SiC as an additional dust component although the formation of SiC is not included in the self-consistent calculations because little is known about the condensation process. While Gauger et al. (1996) find that carbon condenses before SiC, Kozasa et al. (1996) arrive at the opposite conclusion. The effect of α -SiC as dust component is described here in a qualitative manner, i.e. the dust opacity $\chi_d(\nu)$ is calculated from

$$\chi_d = \frac{\chi_C X_C + \chi_{\text{SiC}} X_{\text{SiC}}}{X_C + X_{\text{SiC}}} \quad (1)$$

where X_i are the fractional parts of carbon and SiC, respectively, and where χ_i are the opacities of carbon and SiC in the case of pure grains. To illustrate the influence of α -SiC on the SEDs we have adopted a ratio of $X_C : X_{\text{SiC}} = 4 : 1$ (Lorenz-Martins & Lefèvre 1994, Groenewegen 1995, Ivezić & Elitzur 1995). This mixture of dust grains consisting of amorphous carbon and α -SiC modifies the SED around $11.3 \mu\text{m}$ as shown in Fig. 2.

3.2. Synthetic IRAS colours

We obtain the IRAS colours corresponding to the calculated SEDs by convolving with the IRAS filter transmission curves and by transforming to monochromatic fluxes at $12 \mu\text{m}$, $25 \mu\text{m}$ and $60 \mu\text{m}$ (cf. Joint IRAS Science Work Group, 1986). Fig. 3 depicts self-consistent models at various phases together with black body fluxes (dotted line) and the observations of carbon stars (Guglielmo et al. 1993: small triangles, Kerschbaum & Hron 1994: small diamonds) in the IRAS two-colour diagram with boundaries of certain regions according to van der Veen & Habing (1988). The physical properties of all our theoretical models used in this study are summarized in Table 1. The displacements within a group of symbols are caused by the

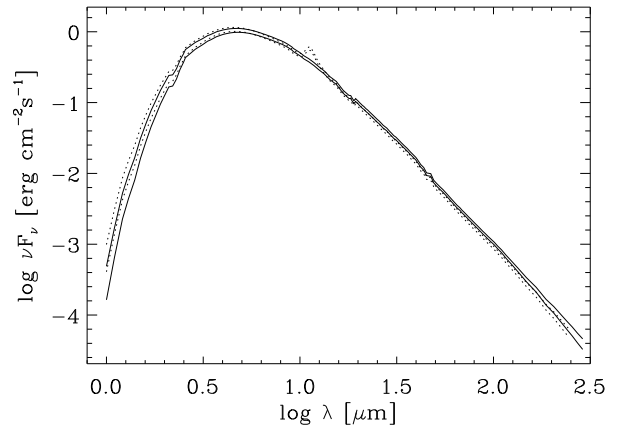


Fig. 2. SEDs for model R10C18 at two different phases with pure amorphous carbon grains (full lines) and with 20 percent of SiC (dotted).

variations during a pulsation cycle and are associated with the time-dependent dust formation and growth processes. Note that based on the measured laboratory data of amorphous carbon (Maron 1990), these IRAS colours can be directly calculated from the extended dynamical models without further assumptions like optical depths, density and temperature structures of the circumstellar envelope, particle size distributions and condensation radii.

The locations of these models in the IRAS two-colour diagram basically reveal a mass loss sequence and are almost independent of the details how the increasing mass loss is generated, i.e. by a different pulsation strength, a lower stellar mass, a higher luminosity or by an increased carbon-to-oxygen ratio. However, the actual position of a model in the two-colour

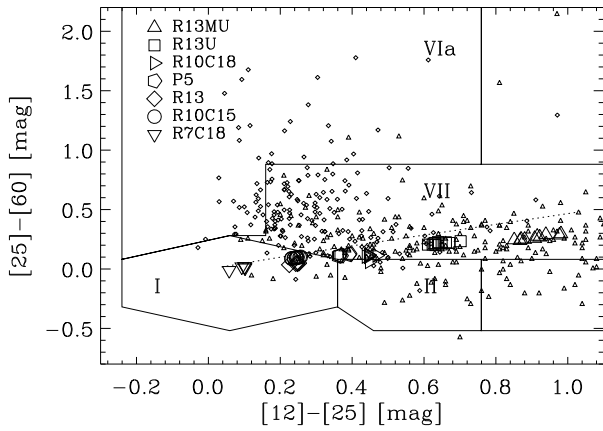


Fig. 3. LPV models at various phases in the IRAS two colour diagram: The symbols correspond to different models and show basically a mass loss sequence where identical symbols belong to various phases of a particular model. The dotted line corresponds to black body fluxes. The small symbols show observed carbon stars (see text).

diagram is phase-dependent and can vary by about 0.2 mag in $[12] - [25]$ colour as well as about 0.1 mag in the $[25] - [60]$ colour. Although we have considered typically ten instants of time for each model covering all pulsational phases the number of symbols which can be distinguished in Fig. 3 depend on specific properties of the model. Some models show similar colours and phases. The maximum light correlates with smallest $[12] - [25]$ and $[25] - [60]$ colours, i.e. both colours increase monotonically with increasing phase. These variations occur within a pulsation and/or dust formation period and are not due to a long term evolution on the AGB like dredge-up phases and He-shell flashes. Therefore, inspecting the mean mass loss rates of the corresponding dynamical models we can relate an observed IRAS source to an estimated mass loss rate but such an estimate is only accurate within a factor of three. Again, we want to emphasize the important influence of the circumstellar envelope on the observed IRAS colours since the mean black body colours of all our initial models constructed with T_* (cf. Table 1) are given for the $[12] - [25]$ colour by 0.098 mag and for the $[25] - [60]$ colour by 0.048 mag.

3.3. Influence of SiC and detached shells

In Fig. 4 we compare the positions of our original models containing amorphous carbon grains (filled symbols) to models that have been modified by the inclusion of additional α -SiC grains (open symbols) and/or of detached shells (which manifest themselves in higher $60 \mu\text{m}$ fluxes as discussed below). The symbols plotted represent mean values (averaged over different phases), except for the stationary model VS.

First, the SiC-feature around $11.3 \mu\text{m}$ results in a shift in both colours which is typically given by 0.2 mag in $[12] - [25]$ and 0.1 mag in $[25] - [60]$. Due to the continuous absorption by SiC this displacement occurs also for models with large mass loss rates ($\dot{M} \simeq 10^{-4} M_{\odot} \text{yr}^{-1}$) where the SiC-feature is not

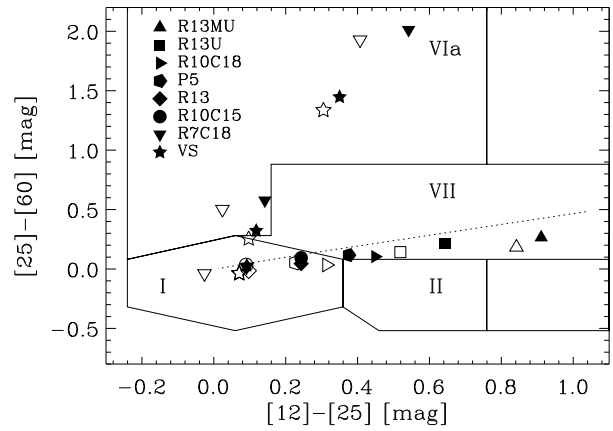


Fig. 4. Influence of SiC and detached shells on the IRAS colours: The full symbols correspond to the extended dynamical models with pure amorphous carbon grains and the open ones to the models with dust particles containing 20 percent SiC grains. In contrast to Fig. 3 only the cycle-averaged value of a model is plotted. The dotted line corresponds to black body fluxes and all models situated distinctly above this line possess detached shells (see text).

visible in the SED anymore. Secondly, the colour shift caused by the inclusion of the SiC dust grains is almost parallel to the model sequence and mimics smaller mass loss rates of models with no SiC dust. An accurate determination of the mass loss rate of a particular object requires therefore the knowledge of a large portion of the SED for several pulsational phases to disentangle the time-dependence of the stellar outflow from the details of the dust forming processes. With IRAS data alone, the effect due to SiC cannot be easily separated from the effects of variations during a pulsational cycle.

We have also simulated the existence of detached shells as found by observations (Olofsson et al. 1990). Without knowing the history of the mass loss and without trying to make ‘realistic’ models we have simply increased the gas and dust densities at a certain radius by a factor of 10 and 100, respectively and have re-done the SED calculations. This radius corresponds to a temperature of typically 100 K which requires a typical flow time of more than 300 years or a few hundred pulsational cycles. The resulting IRAS colours (marked by a star for model VS and by a triangle for model R7C18) are shifted into the regions VIa and VII above the main locations of all our models. The redder $[25] - [60]$ colours correspond to the smaller increase of the mass loss rate, i.e. a factor of 10 in the dust and gas density. Such a detached shell having a temperature of 100 K yields the largest effects on the $60 \mu\text{m}$ flux. Note that both original models are found within region I near (0.1, 0.0) in the IRAS colours.

We regard these simulations of detached shells as numerical experiments to see where an increased mass loss at earlier epochs would shift our dynamical models. We can conclude from varying the parameters of the detached shells that only a rather narrow temperature range around 100 K as well as a mass loss rate increased at least by a factor of 10 is necessary to identify such sources as detached shells in the IRAS database.

3.4. Comparison with observations and previous works

The overall agreement between our synthetic colours and those of observed carbon stars (e.g. Guglielmo et al. 1993) is quite good except that our colours seem to be too blue by about 0.1 mag. This could be due to specific dust properties like the chemical composition or the opacity or due to the small particle limit adopted for this study. Kerschbaum et al. (1996) have made a systematic comparison of the observational properties of carbon-rich Mira, semiregular (SRa and SRb) and irregular (Lb) variables finding that C-Lbs and C-SRabs populate the same areas in the IRAS two colour diagram whereas Miras are separated from them. While the first two groups are mainly found at higher [25]–[60] values in the upper part of region VII and in region VIa, indicating significant amounts of cold dust, the later are located mainly in the lower part of region VII. All variable groups include a small fraction of optically thin objects in the “photospheric” region I extending close to the Rayleigh-Jeans point. Finally, for objects having period information (SRab, Mira) Kerschbaum et al. (1996) have found a positive correlation with the [12]–[25] colour for their samples. When compared with these results, the models without detached shells resemble Mira properties best while the detached shell models are located in regions where mostly semiregular and irregular variables are found. The large fraction of SR and Lb variables among carbon stars with possibly detached shells has already been noted by Willems & de Jong (1988).

Our synthetic colours are similar to the tracks presented by Ivezić & Elitzur (1995) where a parameterized circumstellar envelope is used to model the SEDs of AGB stars. An observable difference is the aforementioned small colour shift. Comparing the mass loss rates, there is an agreement that redder [12]–[25] colours are caused by higher mass loss rates, a result which has also been obtained in earlier investigations (e.g. Chan & Kwok 1990). However, at a given [12]–[25] colour our mass loss rates are significantly larger (factors 2 to 5). The reason for this difference is most likely the effect of pulsation on the density structure of the atmosphere and the complexity of the dust formation process since both aspects are not covered by earlier models. Although it is evident that such kind of parameterized models can reproduce the observed IRAS colours it is very difficult to link the model parameters to actual mass loss rates and other stellar properties.

Using stationary models, Winters et al. (1994a) have presented both synthetic IRAS and near-IR colours. While near IR colours are very useful tools for studying AGB stars (e.g. Epchtein et al. 1990, Kerschbaum & Hron 1994) and well suited to highlight the differences between stationary and dynamical models all modelling requires a proper inclusion of the photospheric radiation. A black body at the inner boundary is apparently not sufficient as can be seen from the systematic differences between observed and synthetic colours found by Winters et al. (1994a) and the difference between blackbody temperatures and effective temperatures (Kerschbaum & Hron 1996). We have therefore concentrated on the IRAS colours

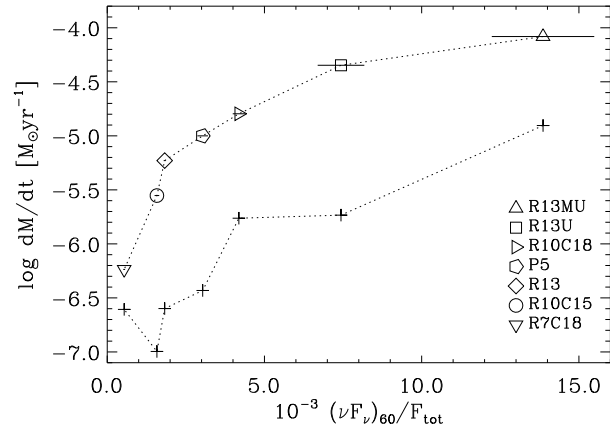


Fig. 5. The mass loss as a function of the 60 μm flux. The symbols correspond to different models and the horizontal bars show the variation during a pulsational cycle. The crosses mark the mass loss according to an empirical mass loss formula by Jura (see text).

while synthetic near IR colours will be the subject of a future paper.

In Fig. 5 we have plotted the mass loss rate against the flux at 60 μm for the dynamical models of Table 1. The horizontal bars give the luminosity and 60 μm flux variations during a pulsational cycle. In order to compare our theoretical mass loss with empirical formulae we adopt Jura’s estimate (Jura 1987) in the version of van der Veen & Olofsson (1989)

$$\dot{M} = 7.7 \cdot 10^{-10} \mu v_{15} D^2 L_4^{-0.5} F_{60} \lambda_{10}^{0.5} \kappa_{\nu,150}^{-1} M_{\odot} \text{ yr}^{-1} \quad (2)$$

where μ is the gas-to-dust ratio, v_{15} the outflow velocity in units of 15 km s⁻¹, D the source distance in kpc, L_4 the luminosity in $10^4 L_{\odot}$, F_{60} the IRAS flux at 60 μm in Jy, λ_{10} the mean wavelength at which the circumstellar envelope emits in units of 10 μm and $\kappa_{\nu,150}$ the dust absorption coefficient at 60 μm in units of 150 cm² g⁻¹. Since all properties needed to evaluate this formula result from our models we have plotted the ‘Jura’ mass loss rates as crosses (joined by a dotted line) for the models using our calculated values for $\kappa_{\nu,150}$ and λ_{10} . We have assumed a source distance of $d = 1$ kpc. The mean emission occurs in our models around $\lambda_{10} \simeq 0.45$, the mean dust absorption coefficient is at $\kappa_{\nu} \simeq 80$ cm² g⁻¹ and the gas-to-dust ratios vary between 277 and 1000 as given in Table 1.

While the general correlation between the mass loss rate and the 60 μm flux contribution is similar for our models and for Jura’s estimate, there are significant systematic differences. These differences can however easily be explained by the fact that for his assumed values for μ and $\kappa_{\nu,150}$ of 220 and 150, respectively he has found good agreement with observed gas mass loss rates. Moreover, his formula is based on several simplifying assumptions like a stationary outflow and small optical depths. This comparison again demonstrates that far-IR observations combined with simple models for the circumstellar envelope can yield realistic mass loss rates but that the properties of the circumstellar envelope may indeed be quite different from the model assumptions.

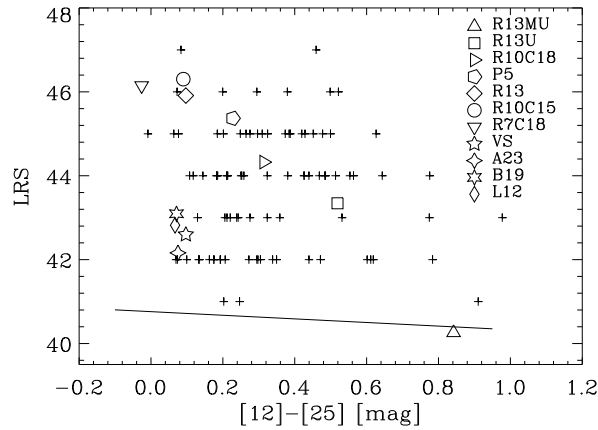


Fig. 6. The IRAS LRS 4n class for the SiC-feature: The theoretical models plotted are in agreement with observed objects (marked by crosses). The solid line at the bottom denotes a linear fit through models without SiC dust.

4. Observed and theoretical IRAS LRS classes

In Kerschbaum et al. (1996) the IRAS LRS classes of the carbon-rich AGB variables have also been investigated with the following result: the ratio of 4n/1n spectra which should be an indicator for the importance of mass loss is for Lbs 1.46, for SRas 1.33, for SRBs 2.44 and for Miras 3.22. Moreover, in the cases of 4n objects the mean classes are 42.7, 43.5, 43.4 and 44.4, respectively. At least for the Miras the trend seems clear that they contain a much larger fraction of higher mass loss objects than the other 3 groups of variables.

For comparison we have plotted the LRS classes of known, carbon-rich variables together with our models containing amorphous carbon particles as well as α -SiC grains (in the ratio of 4:1). Fig. 6 depicts the IRAS LRS 4n class according to the definitions of the Joint IRAS Science Working Group (1988) as a function of the [12]–[25] colour where the LRS class characterizes the strength of the SiC-feature around $11.3 \mu\text{m}$. The solid line at the bottom of the plot denotes a linear fit through all models without SiC-dust. Hence, we expect all observations above this line. For clarity we plot only the time-averaged values of the dynamical models. At most we find a change of one LRS class over time. Our dynamical models form a nearly linear sequence through the bulk of the observations of carbon-rich Miras, SRa-, SRb- and Lb- variables plotted as small crosses. The agreement between observations and models would be even better if the slight colour shift noted in the two-colour diagram is taken into account. The small number of observed stars at small LRS classes and red [12]–[25] colours is probably due to an observational bias against the detection of variability for stars with high mass loss rates (Guglielmo et al. 1993).

All stationary dust-driven outflows (models VS, A23, B19 and L12) are concentrated around an LRS class of 43 with a [12]–[25] value of about 0.1. These symbols together with model R7C18 correspond nicely to the left boundary seen in the observations. Note that these bluest models exhibit also the

smallest mass loss rates of our theoretical sample (cf. Table 1). The plot thus indicates that dynamical models have a higher LRS class at a given mass loss rate than the stationary ones.

If the stationary models are associated with stars with small pulsation amplitudes and/or irregular variability, the observed blue objects with weak LRS features should thus all be such stars. Indeed this is seen in the pulsation characteristics of the observed stars. However, large amplitude variables can also show blue IRAS colours and a weak SiC feature, indicating that the pulsation amplitude and regularity alone are not sufficient to distinguish between time-dependent and stationary cases.

5. Discussion and conclusions

Concerning the nature of these synthetic IRAS colours calculated from self-consistent models of dust-driven winds, several points need to be emphasized. First, in contrast to scalable models (e.g. Ivezić & Elitzur 1995) where e.g. the condensation temperature and the properties of the dust grains have to be specified or where the relation of important quantities like mass loss rates and outflow velocities to fundamental stellar parameters is uncertain due to simplifying assumptions and adjustable parameters of the models, we can calculate the entire dynamical structure of the outflow depending only on fundamental stellar parameters. Secondly, while the outer structure of the stellar mass loss visible in the [25]–[60] colour can be represented by time-integrated properties the results of our dynamical models show that the [12]–[25] fluxes generated much closer to the star are strongly influenced by short time dynamical phenomena like pulsations, shocks and time-dependent dust formation.

Comparing our self-consistent models with mass loss estimates like (e.g. Ivezić & Elitzur 1995)

$$\dot{M} u_\infty = \tau_F \frac{L_\star}{c} \left(1 - \frac{1}{\Gamma} \right) \quad (3)$$

reveals a number of basic differences. Here $\tau_F = \int \tau_\lambda F_\lambda d\lambda / \int F_\lambda d\lambda$ denotes the flux-weighted optical depth and Γ the spatially integrated ratio between gravitational and radiative acceleration. In our models we have not assumed a certain condensation point but calculated the extended zone where dust particles condense and grow to their final sizes. It is difficult to define an appropriate inner boundary for the spatial integration. The value of Γ clearly depends on this point and approaches unity as the boundary is shifted inwards. Furthermore the formula given above is derived for stationary outflows driven by radiation pressure neglecting the momentum input by stellar pulsations. Hence, our LPV models are not consistent with this kind of relation and we obtain negative values of Γ for certain models. As demonstrated in Höfner & Dorfi (1997) the outflow velocities of the models show a good correlation with a quantity which characterizes the strength of radiation pressure on dust relative to gravitation whereas no such correlation is found for the mass loss rate or $\dot{M} u_\infty$.

We want to express a general warning that fitting the observed quantities by an assumed stationary outflow can lead to severe problems because the variations in the [12]–[25]

fluxes occurring during a pulsational cycle are then extrapolated through the whole circumstellar envelope up to several thousand stellar radii. At large distances the stellar outflow becomes more and more stationary but the inner part of the wind zone is totally dominated by the time-dependence of the dust formation process. Hence, within a few photospheric radii the density, temperature and velocity structure is completely different from a stationary solution. Using stationary models may therefore result in relations between quantities characterizing the outflow (like mass loss rates and outflow velocities or dust-to-gas ratios) and intrinsic stellar properties (luminosity, mass, chemical abundances, etc.) which are seriously wrong.

Based on the IRAS observations it has been pointed out earlier (van der Veen & Habing 1988) that the location of an object in the IRAS two colour diagram represents basically the mass loss rate. Our theoretical models of dust driven winds support this conclusion and show that the specific stellar conditions (luminosity, stellar mass, carbon-to-oxygen ratio, etc.) causing a certain mass loss cannot be easily extracted from such a diagram because the mass loss rate depends on the stellar parameters in a complicated, non-unique way.

Concerning the simulations of detached shells and dust grains containing SiC we have demonstrated how the structure and composition of the dust envelope affects the position in this IRAS diagram.

Acknowledgements. This work is supported by the *Fonds zur Förderung der wissenschaftlichen Forschung (FWF)*, projects S7305–AST, S7308–AST and J01283–AST. We thank the referee Dr. M.A.T. Groenewegen for valuable comments on the manuscript.

References

- Chan S.J., Kwok S. 1990, A&A 237, 354
 Dorfi E.A., Höfner S. 1996, A&A, 313, 605
 Epchtein N., Le Bertre T., Lépine J.R.D., 1990, A&A 227, 82
 Fleischer A. J., Gauger A., Sedlmayr E. 1991, A&A 242, L1
 Fleischer A. J., Gauger A., Sedlmayr E. 1992, A&A 266, 321
 Fleischer A. J., Gauger A., Sedlmayr E. 1995, A&A 297, 543
 Gail H.-P., Sedlmayr E. 1988, A&A 206, 153
 Gauger A., Gail H.-P., Sedlmayr E. 1990, A&A 235, 345
 Gauger A., Keady J.J., Sedlmayr E. 1996, In: Proc. IAU Symp. 177, The Carbon Star Phenomenon, Kluwer Acad. Publ., Dordrecht, in press
 Groenewegen M.A.T. 1995, A&A 293, 463
 Guglielmo F., Epchtein N., Le Bertre T., et al. 1993, A&AS 99, 31
 Habing H.J. 1996, A&AR 7, 97
 Höfner S., Feuchtinger M., Dorfi E.A. 1995, A&A 297, 815
 Höfner S., Fleischer A.J., Gauger A., et al. 1996, A&A, 314, 204
 Höfner S., Dorfi E.A. 1997, A&A 319, 648
 Ivezić Ž., Elitzur M. 1995, ApJ 445, 415
 Joint IRAS Science Working Group, 1986, IRAS Catalogs and Atlases, IRAS Atlas of low-resolution Spectra, A&AS 65, 607 (**IRAS-LRS**)
 Joint IRAS Science Working Group, 1988, IRAS Catalogs and Atlases, Volume 1: Explanatory Supplement, NASA RP-1190 (**IRAS-EXP**)
 Jura M. 1987, ApJ 313, 743
 Kerschbaum F., Hron J. 1994, A&AS 106, 397
 Kerschbaum F., Hron J. 1996, A&A 308, 489

- Kerschbaum F., Habison P., Hron J., Loidl R., Olofsson H. 1996, In: Proc. IAU Symp. 177, The Carbon Star Phenomenon, Kluwer Acad. Publ., Dordrecht, in press
 Kozasa T., Dorschner J., Henning T., Stognienko R. 1996, A&A 307, 551
 Lorenz-Martins S., Lefèvre J. 1994, A&A 291, 831
 Lucy L. 1971, ApJ 163, 95
 Lucy L. 1976, ApJ 205, 482
 Maron N. 1990, Ap&SS 172, 21
 Olofsson H., Carlström U., Eriksson K., et al. 1990, A&A 230, L13
 Pégourié B. 1988, A&A 194, 335
 Rowan-Robinson M., Harris S. 1983, MNRAS 202, 797
 Speck A.K., Barlow M.J., Skinner C.J. 1996, In: Proc. IAU Symp. 177, The Carbon Star Phenomenon, Kluwer Acad. Publ., Dordrecht, in press
 van der Veen W.E.C.J., Habing H.J. 1988, A&A 194, 125
 van der Veen W.E.C.J., Olofsson, H. 1989 In: From Miras to Planetary Nebulae: Which Path for Stellar Evolution?, Eds. M.O. Mennessier and A.Omont, Editiones Frontières, Montpellier 1989, p. 149
 Willems F.J., de Jong T., 1988, A&A 196, 173
 Winters J.M., Dominik C., Sedlmayr E. 1994a, A&A 288, 255
 Winters J.M., Fleischer A.J., Gauger A., Sedlmayr E. 1994b, A&A 290, 623
 Winters J.M., Fleischer A.J., Gauger A., Sedlmayr E. 1995, A&A 302, 483
 Yorke H.W. 1980, A&A 86, 286